Supplementary Materials and Methods.

Amnis ImageStream Flow cytometry. Imagestream, which combines high-throughput advantages of flow cytometry with morphological and fluorescence features derived from microscopy is a powerful tool to analyze chromatin condensation in a single cell manner[1]. To examine chromatin condensation, 1 x 10^6 sorted erythroblasts were stained with APC-conjugated mouse human GPA and Hoechst 33342 for 20 minutes at room temperature. To observe the relationship between acetylated histone 4 (Ac-H4) and chromatin condensation, 1 x 10^6 of sorted erythroblasts were fixed in 4% paraformaldehyde in PBS at 4°C overnight. The fixed cells were re-suspended in 100 μl of PBS-T (PBS containing 1% BSA, 0.1% Triton-X100, 10% normal goat serum) for 20 minutes at room temperature for cell permeabilization and for blocking of non-specific binding. The cells were then incubated with mouse anti-Ac-H4 (1:100 diluted in PBS-T) for 2 hours at room temperature, followed by incubation with AF-488-conjugated goat anti-mouse IgG (1:1000 diluted in PBS-T), APC-conjugated mouse anti-human GPA and Hoechst 33342 for 1 hour in dark at room temperature. After washing, the cells were re-suspended in 50μl PBS, and immediately subjected to Amnis ImageStream analysis. Data was collected on an Amnis ImageStream Mark II instrument using a 60 X objective. IDEAS software was used to analyze the data.

Co-immunoprecipitation. Human erythroleukemia cell line K562 was grown in RPMI-1640 medium (Sigma) supplemented with 10% fetal bovine serum (Hyclone), penicillin-streptomycin (Thermo Fisher Scientific) at 37℃ in 5% CO_2. 50 x10^6 cells were harvested and lysed with RIPA Lysis and Extraction Buffer (Thermo Fisher Scientific) for 60 minutes on ice. Supernatant was collected following centrifugation at 14,000 g at 4°C for 10 minutes and the concentration of protein in the supernatant was determined as previously described[2]. The co-immunoprecipitation was performed as previously described using anti-histone 4 or anti-HDAC5 antibody[3–5].

RNA-seq and ATAC-seq. RNA was extracted from FACS-sorted polychromatic and orthochromatic erythroblasts following HDAC5 knockdown. Approximately 100 ng of total RNA was used as input for cDNA library preparation, which was preformed using an Illumina TruSeq kit followed by sequencing using an Illumina HiSeq 4000 platform (Beijing Genomics Institute, BGI, China). The luciferase controls of bulk-RNA-seq data of polychromatic and orthochromatic erythroblasts were from our previous report[6]. For analysis of RNA-seq data, gene read counts for gencode hg19 version 31 protein coding genes were generated using kallisto[7]. Differential gene expression was examined utilizing DESeq2[8] using a Wald test where the log2 fold change is greater than 0.5 with a 0.05 adjusted p-value cutoff and independent filtering to remove genes with lower expression levels. Overrepresented gene ontology biological process terms were identified using the clusterProfiler package with q-value <0.05[9]. Assay for Transposase-Accessible Chromatin Sequencing (ATAC-seq) was performed according to the published omni-ATAC protocol[10]. Briefly, nuclei were extracted from

50,000 cells of FACS-sorted polychromatic or orthochromatic erythroblasts following HDAC5 knockdown or luciferase control, followed by the transposition reaction performed with Tn5 transposase. The transposed DNA was purified and amplified to generate sequencing libraries following manufacturer instructions (Nextera DNA Library Prep Kit, FC-121-1030). Amplified DNA fragments from 150bp to 1000bp range were purified and sequenced by Illumina HiSeq 4000 with 100bp pair-end runs. Sequencing reads were trimmed using trimmomatic to remove adapters, and then mapped to the hg19 genome using bwa-mem[11]. Reads mapping to ENCODE blacklist regions and the mitochondrial genome, and reads that did not map uniquely were removed. Peaks were called using MACS2 using parameters --nomodel --shift -100 --extsize 200[12]. Differentially bound peaks were identified using the DiffBind package[13] after removing weakly bound regions with filter value of 150 using the DESEQ2 method, FDR threshold of .01 and fold change of 2, normalizing to the number of reads in the full library. Peaks were annotated to the nearest gene transcription start site for comparison with gene expression using the ChIPseeker package[14].

REFERENCES

1. Swartz KL, Wood SN, Murthy T, et al. E2F-2 Promotes Nuclear Condensation and Enucleation of Terminally Differentiated Erythroblasts. *Mol. Cell. Biol.* 2017;37(1):.

2. Chen K, Liu J, Heck S, et al. Resolving the distinct stages in erythroid differentiation based on dynamic changes in membrane protein expression during erythropoiesis. *Proc. Natl. Acad. Sci.* 2009;106(41):17413–17418.

3. Chen L, Wang T, Wang Y, et al. Protein 4.1G regulates cell adhesion, spreading, and migration of mouse embryonic fibroblasts through the β1 integrin pathway. *J. Biol. Chem.* 2016;291(5):2170–2180.

4. Wang Y, Zhang H, Kang Q, et al. Protein 4.1N is required for the formation of the lateral membrane domain in human bronchial epithelial cells. *Biochim. Biophys. Acta - Biomembr.* 2018;1860(5):1143–1151.

5. Liang L, Peng Y, Zhang J, et al. Deubiquitylase USP7 regulates human terminal erythroid differentiation by stabilizing GATA1. *Haematologica*. 2019;104(11):2178–2188.

6. Huang Y, Hale J, Wang Y, et al. SF3B1 deficiency impairs human erythropoiesis via activation of p53 pathway: Implications for understanding of ineffective erythropoiesis in MDS. *J. Hematol. Oncol.* 2018;11(1):19.

7. Bray NL, Pimentel H, Melsted P, Pachter L. Near-optimal probabilistic RNA-seq quantification. *Nat.*

Biotechnol. 2016;34(5):525–527.

8. Love MI, Huber W, Anders S. Moderated estimation of fold change and dispersion for RNA-seq data with DESeq2. *Genome Biol.* 2014;15(12):550.

9. Yu G, Wang LG, Han Y, He QY. ClusterProfiler: An R package for comparing biological themes among gene clusters. *Omi. A J. Integr. Biol.* 2012;16(5):284–287.

10. Buenrostro JD, Wu B, Chang HY, Greenleaf WJ. ATAC-seq: A method for assaying chromatin accessibility genome-wide. *Curr. Protoc. Mol. Biol.* 2015;2015:21.29.1-21.29.9.

11. Li H, Durbin R. Fast and accurate short read alignment with Burrows-Wheeler transform. *Bioinformatics*. 2009;25(14):1754–1760.

12. Zhang Y, Liu T, Meyer CA, et al. Model-based analysis of ChIP-Seq (MACS). *Genome Biol.* 2008;9(9):R137.

13. Ross-Innes CS, Stark R, Teschendorff AE, et al. Differential oestrogen receptor binding is associated with clinical outcome in breast cancer. *Nature*. 2012;481(7381):389–393.

14. Yu G, Wang LG, He QY. ChIP seeker: An R/Bioconductor package for ChIP peak annotation, comparison and visualization. *Bioinformatics*. 2015;31(14):2382–2383.

Supplementary figure legends

Fig S1. HDAC5 shRNAs had no effects on the expression of HDACs. qRT-PCR results showing relative mRNA levels of HDAC1, 2, 3, 6 and 7 in sorted control and HDAC5-knockdown erythroblasts. β-actin was used as internal reference for the qRT-PCR.

Fig S2. Cytospin images of shLuci and shHDAC5 transduced polychromatic and orthochromatic erythroblasts. Composite representative cytospin images of shLuci and shHDAC5 transduced polychromatic **(A)** and orthochromatic erythroblasts **(B)**. Scale bar:10μm.

Fig S3. Co-immunoprecipitation of histone 4 and HDAC5. (A) Representative western blots following immunoprecipitation with anti-histone 4 antibody. **(B)** Representative western blots of following immunoprecipitation with anti-HDAC5 antibody.

Fig S4. siRNA mediated-HDAC5 knockdown leads to increased apoptosis of late stage erythroblasts due to activation of p53 pathway. Cells were transfected on day 9 and assessed on day 11. **(A)** Schematic diagram of target regions of shRNAs and siRNAs. **(B)** qRT-PCR results showing HDAC5 mRNA levels. β-actin was used as internal reference. **(C)** Representative western blotting showing HDAC5 protein levels. **(D)** Quantitative analyses of HDAC5 protein levels. **(E)** Growth curves. **(F)** Quantitative analysis of apoptosis. **(G)** Representative western blots of molecules as indicated. **(H)** Quantitative analyses of western blotting results. **(I)** Effects of HDAC5 siRNAs on the expression of other HDACs as indicated. N=3. ** $p<0.01$, *** $p<0.001$.

Fig S5. Effects of siRNA-mediated HDAC5 knockdown on enucleation, chromatin condensation and H4 acetylation. (A) through (G): cells were transfected on day 13 and assessed on day 15. **(H) through (N):** cells were transfected on day 15 and assessed on day 17. **(A) and (H)** qRT-PCR showing HDAC5 mRNA expression levels. **(B) and (I)** Representative western blotting showing HDAC5 protein levels. **(C) and (J)** Quantitative analyses of HDAC5 protein levels. **(D) and (K)** Quantitative analysis of enucleation rate. **(E) and (L)** Quantitative analysis of nuclear diameter. **(F) and (M)** Representative western blotting showing H4 acetylation at K5 and K12. **(G) and (N)** Quantitative analyses of H4 acetylation at K5 and K12. **(O)** Effects of HDAC5 siRNAs on the expression of other HDACs as indicated. N=3. * $p<0.01$, ** $p<0.01$, *** $p<0.001$.

Fig S6. Effect of LMK235 on erythroblast enucleation. (A) Representative profiles of enucleation as assessed by Syto16 staining on day 14 of culture. Enucleation percentage was calculated as Syto16 negative population in total population. **(B)** Quantitative analysis of enucleation. N=3. *** $p<0.001$.

Fig S7. LMK235 had no effect on H4 acetylation at K5 and K8. (A) Representative western blots showing acetylation of H4(K5). **(B)** Quantitative analyses of acetylation of H4(K)5. **(C)** Representative western blots showing acetylation of H4 (K8). **(D)** Quantitative analyses of acetylation of H4(K8). N=3.

Fig S8. HDAC6 inhibitor Tubacin had no effect of on H4 acetylation. (A) Representative western blots showing H4 (K5) acetylation. **(B)** Quantitative analyses of H4(K5) acetylation. **(C)** Representative western blots showing H4 (K8) acetylation. **(D)** Quantitative analyses of H4(K8) acetylation. **(E)** Representative western blots showing H4 (K12) acetylation. **(F)** Quantitative analyses of H4(K12) acetylation.

Fig S1

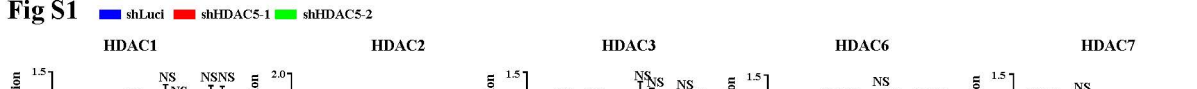
shLuci
shHDAC5-1
shHDAC5-2
HDAC1
HDAC2
HDAC3
HDAC6
HDAC7
Relative mRNA expression
Pro
Baso
Poly
Ortho
NS

Fig S2

A

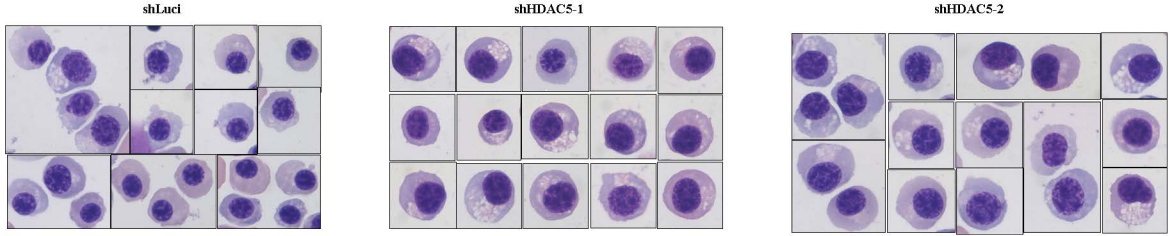

B

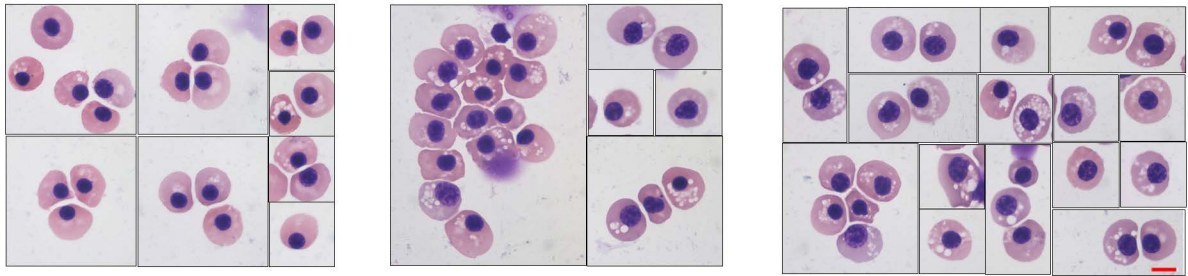

Fig S3

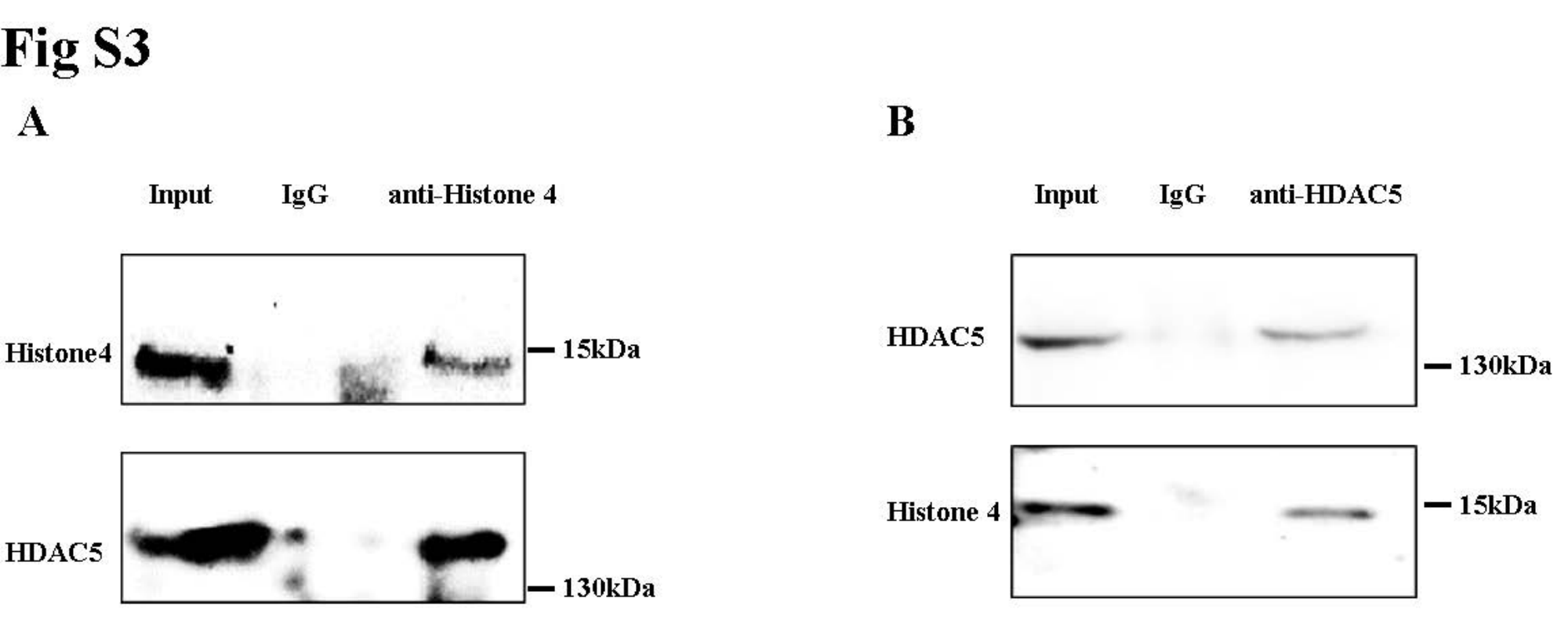
A
Input
IgG
anti-Histone 4
Histone4
15kDa
HDAC5
130kDa
B
Input
IgG
anti-HDAC5
HDAC5
130kDa
Histone 4
15kDa

Fig S4

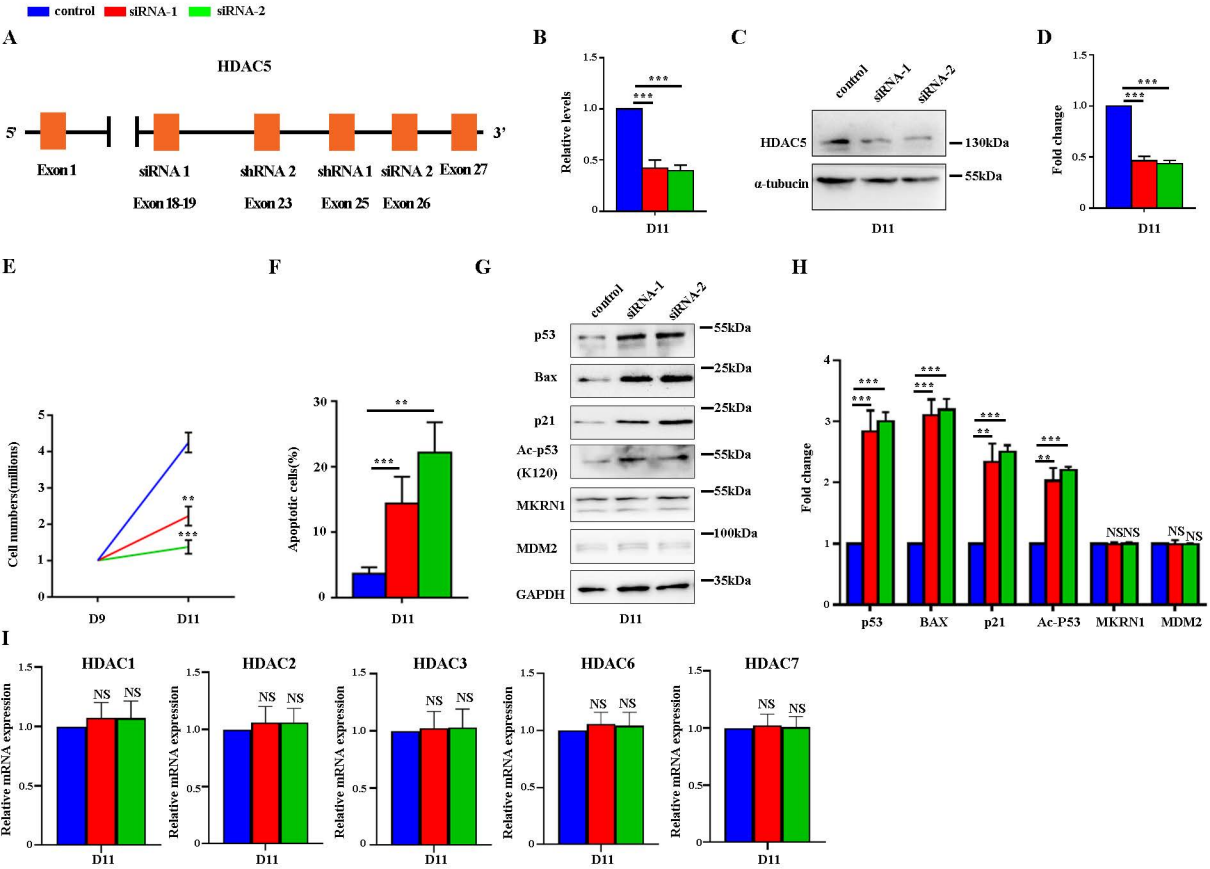
control
siRNA-1
siRNA-2
A
HDAC5
5'
3'
Exon 1
siRNA 1
Exon 18-19
shRNA 2
Exon 23
shRNA 1
Exon 25
siRNA 2
Exon 26
Exon 27
B
Relative levels
D11
C
control
siRNA-1
siRNA-2
HDAC5
130kDa
α-tubucin
55kDa
D11
D
Fold change
D11
E
Cell numbers(millions)
D9
D11
F
Apoptotic cells(%)
D11
G
control
siRNA-1
siRNA-2
p53
55kDa
Bax
25kDa
p21
25kDa
Ac-p53
(K120)
55kDa
MKRN1
55kDa
MDM2
100kDa
GAPDH
35kDa
D11
H
Fold change
NS
p53
BAX
p21
Ac-P53
MKRN1
MDM2
I
HDAC1
HDAC2
HDAC3
HDAC6
HDAC7
Relative mRNA expression
NS
D11

Fig S5

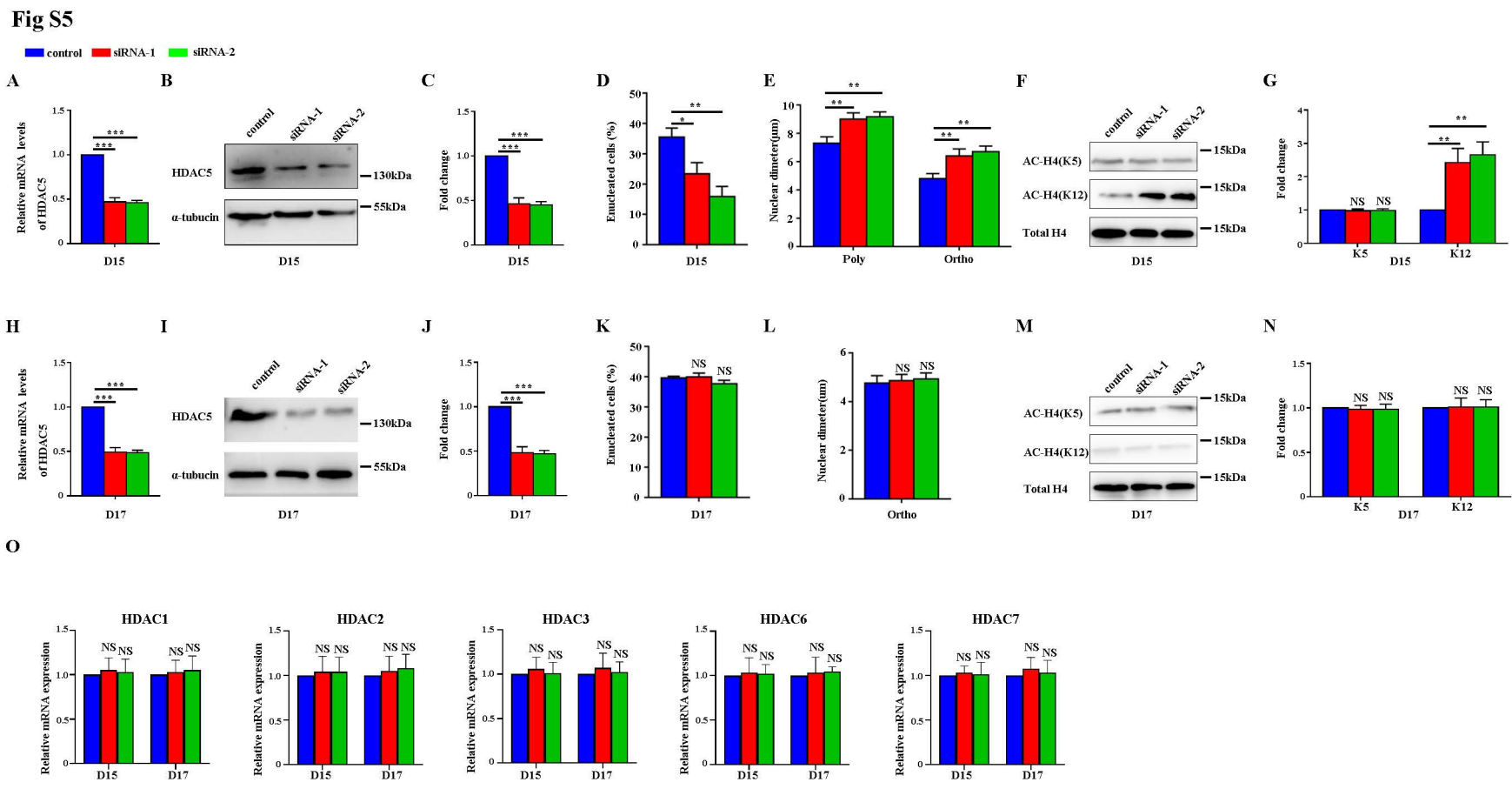
control
siRNA-1
siRNA-2
A
B
C
D
E
F
G
H
I
J
K
L
M
N
O
Relative mRNA levels of HDAC5
HDAC5
α-tubucin
130kDa
55kDa
Fold change
Enucleated cells (%)
Nuclear dimeter(um)
Poly
Ortho
AC-H4(K5)
AC-H4(K12)
Total H4
15kDa
K5
K12
NS
D15
D17
HDAC1
HDAC2
HDAC3
HDAC6
HDAC7
Relative mRNA expression

Fig S6

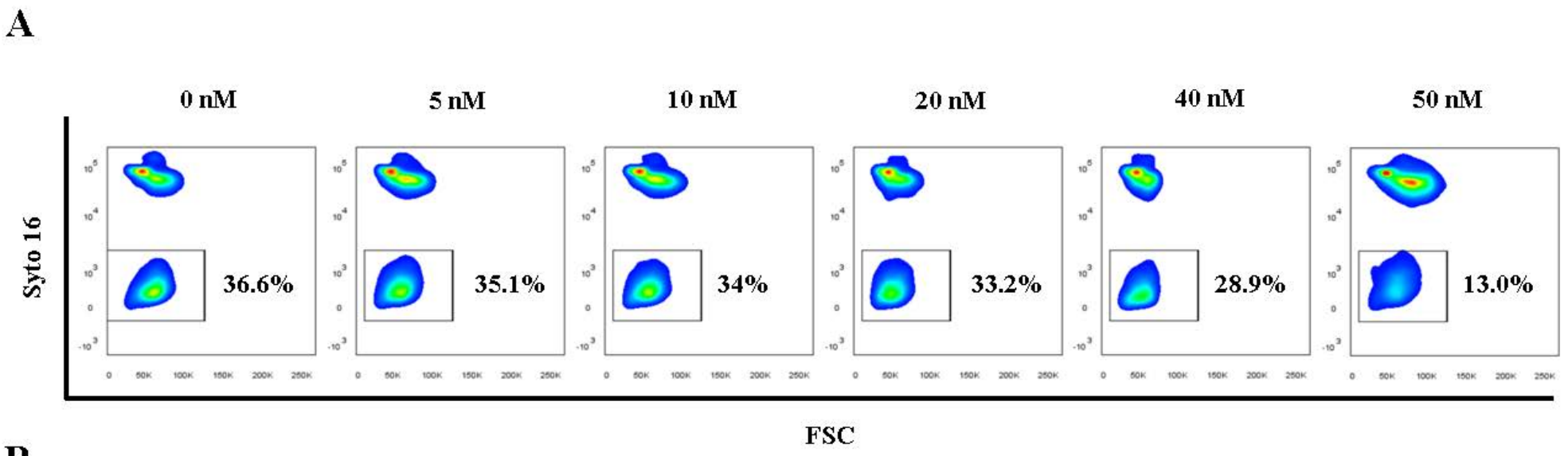
A
0 nM
5 nM
10 nM
20 nM
40 nM
50 nM
Syto 16
36.6%
35.1%
34%
33.2%
28.9%
13.0%
FSC
B
***
NS
NS
NS
NS
1.5
1.0
0.5
0
Fold change of Enucleated cells
D14
LMK235
0 nM
5 nM
10 nM
20 nM
40 nM
50 nM

Fig S7

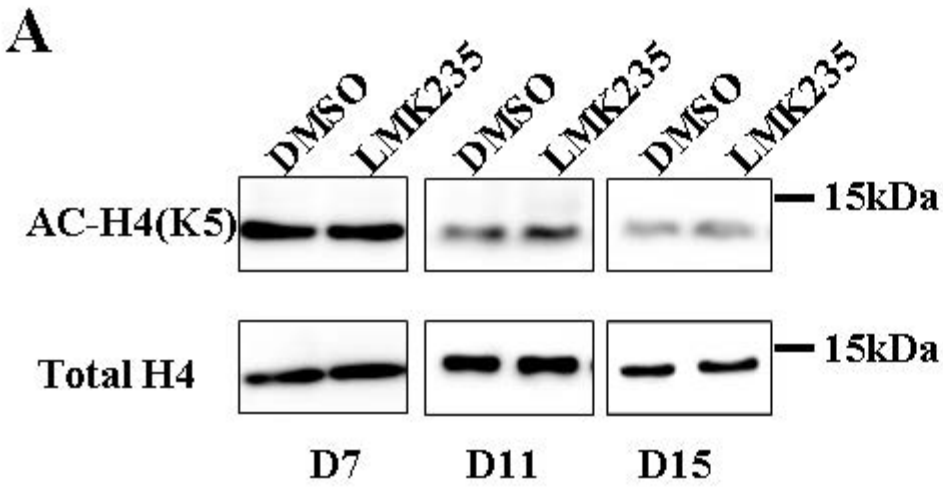
A
DMSO
LMK235
DMSO
LMK235
DMSO
LMK235
AC-H4(K5)
15kDa
Total H4
15kDa
D7
D11
D15

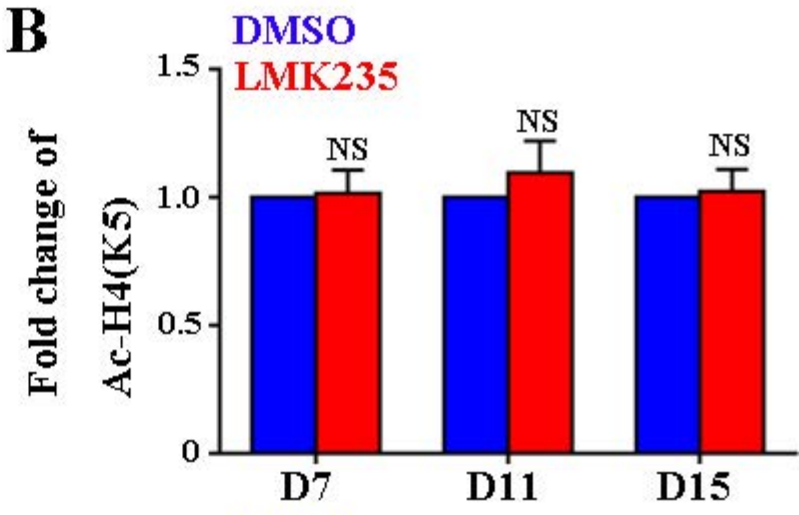
B
DMSO
LMK235
Fold change of Ac-H4(K5)
1.5
1.0
0.5
0
NS
NS
NS
D7
D11
D15

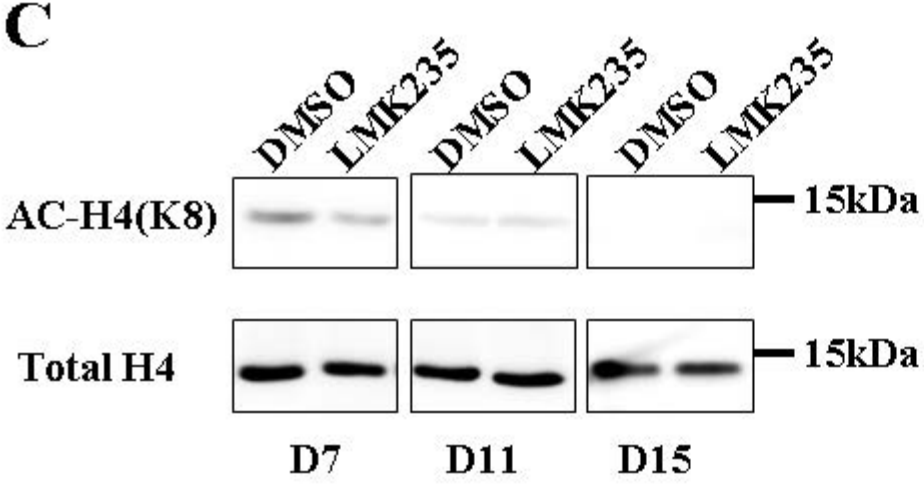
C
DMSO
LMK235
DMSO
LMK235
DMSO
LMK235
AC-H4(K8)
15kDa
Total H4
15kDa
D7
D11
D15

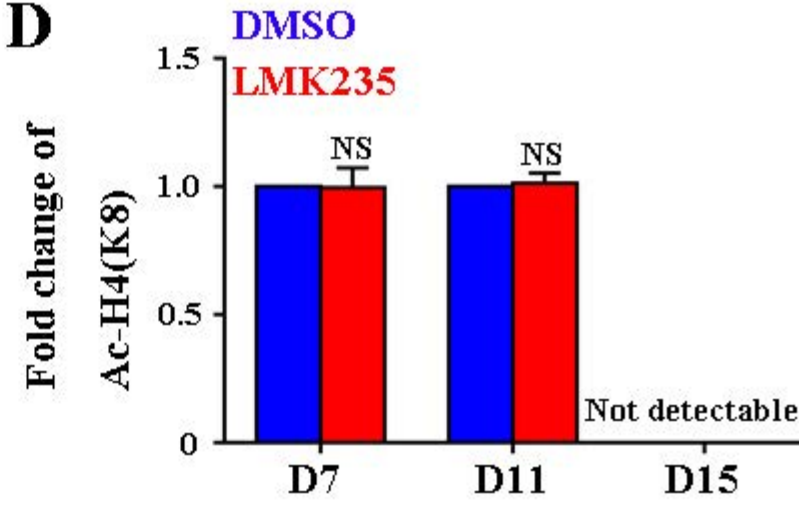
D
DMSO
LMK235
Fold change of Ac-H4(K8)
1.5
1.0
0.5
0
NS
NS
Not detectable
D7
D11
D15

Fig S8

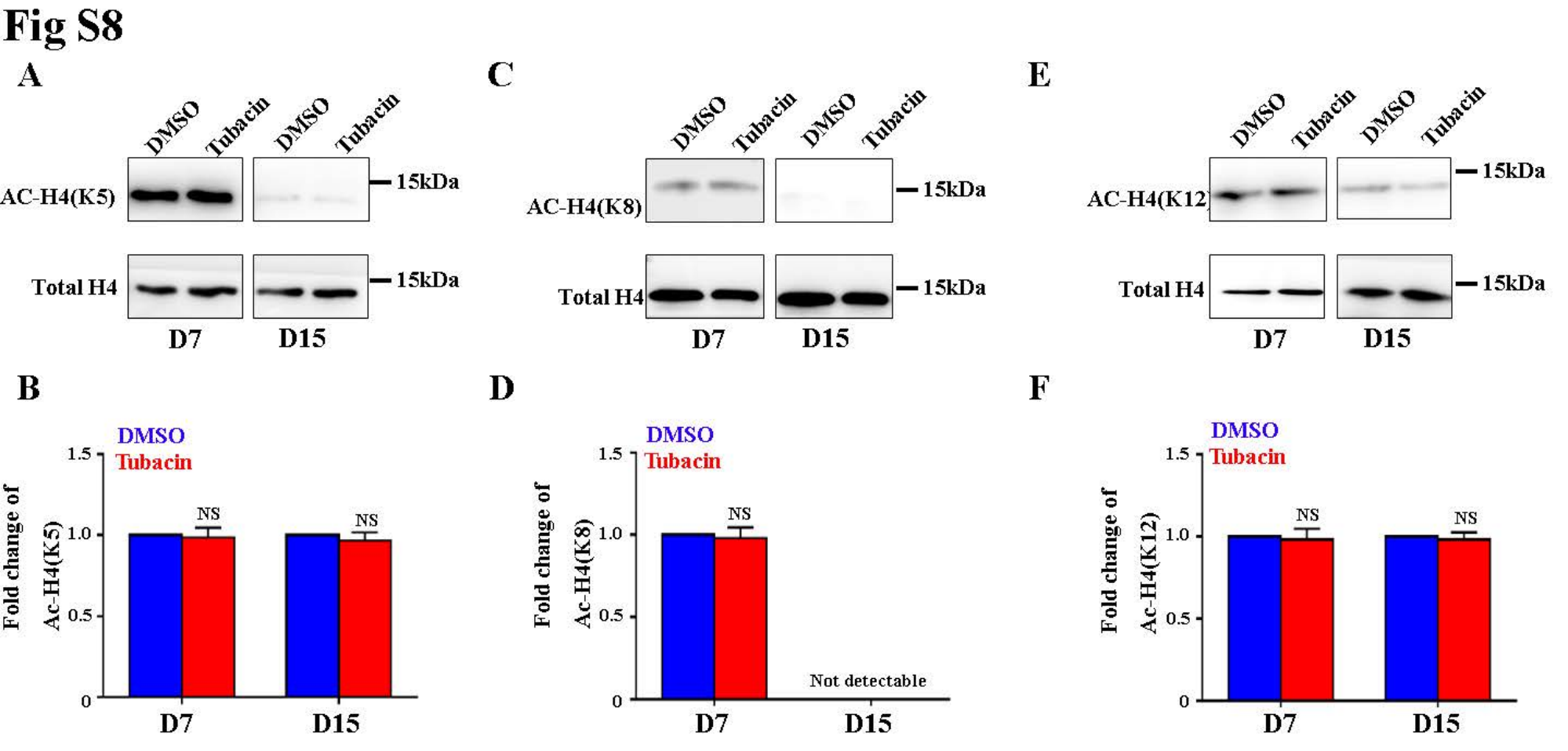
A
DMSO
Tubacin
DMSO
Tubacin
AC-H4(K5)
15kDa
Total H4
15kDa
D7
D15
C
DMSO
Tubacin
DMSO
Tubacin
AC-H4(K8)
15kDa
Total H4
15kDa
D7
D15
E
DMSO
Tubacin
DMSO
Tubacin
AC-H4(K12)
15kDa
Total H4
15kDa
D7
D15
B
DMSO
Tubacin
Fold change of Ac-H4(K5)
1.5
1.0
0.5
0
NS
NS
D7
D15
D
DMSO
Tubacin
Fold change of Ac-H4(K8)
1.5
1.0
0.5
0
NS
Not detectable
D7
D15
F
DMSO
Tubacin
Fold change of Ac-H4(K12)
1.5
1.0
0.5
0
NS
NS
D7
D15